Microchimica Acta (2024) 191:89
https://doi.org/10.1007/s00604-023-06144-9

ORIGINAL PAPER

A photoelectrochemical aptasensing platform assembled at the heterojunction interface of Cu_3BiS_3 sensitized CuV_2O_6 for bisphenol A

Han Meng[1] · Rui Xu[1] · Kun Xu[1] · Dongquan Leng[1] · Lei Liu[1] · Huangxian Ju[1] · Xuejing Liu[1] · Qin Wei[1,2]

Received: 20 September 2023 / Accepted: 6 December 2023 / Published online: 11 January 2024

Abstract

The interaction between the sensitive interfaces of photoelectrochemical (PEC) semiconductor nanomaterials and microscopic matter creates endless potential for the efficient detection of endocrine disruptor. This work presents the development of a high-efficiency PEC aptasensor for bisphenol A (BPA) monitoring based on Cu_3BiS_3 sensitized CuV_2O_6 nanocomposites with exceptional visible-light PEC activity. We implemented the integration of Cu_3BiS_3 nanosheet photosensitizer to sensitize the CuV_2O_6 nanowire structure that was synthesized utilizing a facile hydrothermal approach. The band gap alignment between Cu_3BiS_3 and CuV_2O_6 facilitated enduring PEC response yielding an efficient interfacial structure. The surface of the CuV_2O_6/Cu_3BiS_3 electrode was modified with BPA aptamer, enabling specific binding with BPA and precise quantification of its content. The developed aptamer sensors possess a wide detection range of 5.00×10^{-1} to 5.00×10^{4} ng/mL, and a low detection limit of 1.60×10^{-1} ng/mL (at $S/N = 3$). After undergoing 20 testing cycles and enduring long-term storage, the sensor maintained its stability and showcased excellent repeatability and reproducibility. This study presents a promising methodology for the detection of BPA in environmental settings.

Keywords Photoelectrochemistry · Environmental monitoring · Cu_3BiS_3/CuV_2O_6 · Nanosheets · Bisphenol A · Aptasensor

Introduction

Bisphenol A (BPA) is an essential industrial organic agent in the world; it is widely used in the production of epoxy resins and polycarbonate [1]. As a result, a large amount of BPA remains in the ecological environment. However, excessive use of BPA may cause many health hazards [2], including cardiovascular disease [3], immune impairment [4], breast tumors, and obesity [5]. The European Union's 2018/213 test standard dictates that the quantity of BPA allowed in varnishes or coatings should not exceed 0.05 mg/kg. Furthermore, BPA should not be present in any materials or items that may come into contact with baby food or comparable foodstuffs [6]. Hence, there is an urgent requirement to create a new method that can be sensitively and effectively detected BPA to reduce its harmful effects on humans. In recent years, many ways have been successfully used for BPA detection [7], such as fluorescence assay [8], electrochemiluminescence [9], and electrochemical method [10]. They have the advantages of wide detection range and high sensitivity. Among them, electrochemical detection is widely used for PBA detection due to the advantages of simple operation and miniaturization. However, electrochemical oxidation of PBA often generates a polymer on the electrode surface, which prevents the enhancement of electrode sensitivity by causing electrode passivation [11]. Thus, it is of great significance to find a sensitive and convenient method to realize the detection of BPA. Photoelectrochemical (PEC) sensors address the limitations of the above methods and also have the advantages of easy operation and low energy consumption [12, 13]. In short, PEC sensors work by

Han Meng and Rui Xu contributed equally to this work.

✉ Xuejing Liu
chm_liuxj@ujn.edu.cn

✉ Qin Wei
sdjndxwq@163.com

[1] Key Laboratory of Interfacial Reaction & Sensing Analysis in Universities of Shandong, School of Chemistry and Chemical Engineering, University of Jinan, Jinan 250022, People's Republic of China

[2] Department of Chemistry, Sungkyunkwan University, Suwon 16419, Republic of Korea

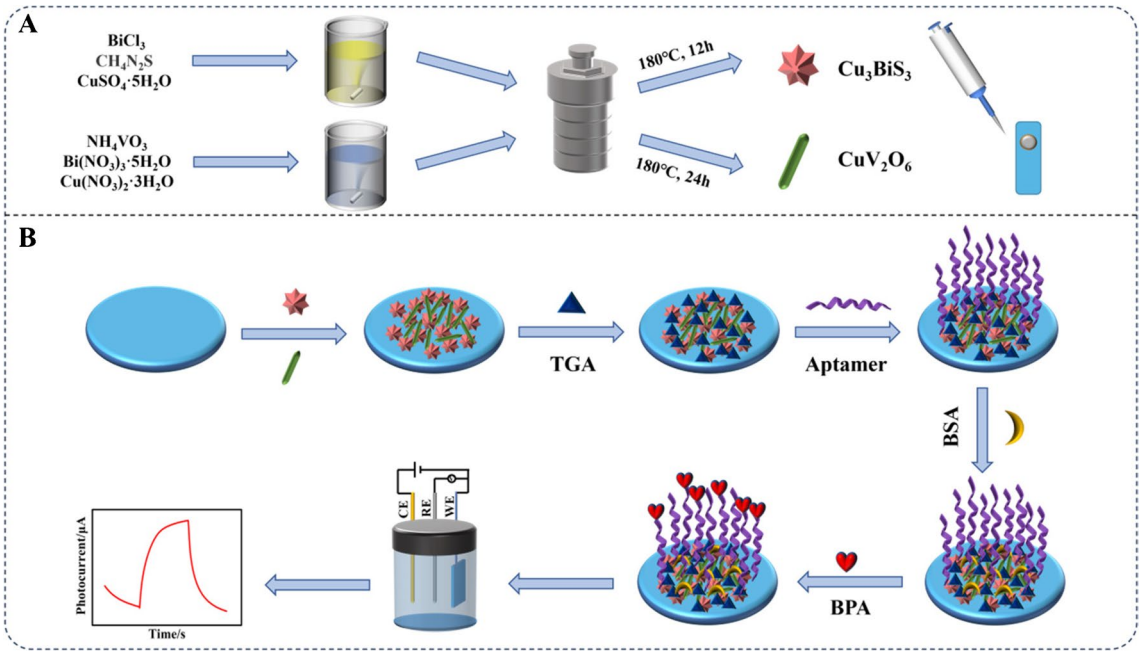

Scheme 1 Schematic diagram of the construction process of the PEC aptasensor

transferring photoelectrons from photosensitive materials to electrodes or solutions when they are excited by light, resulting in a readable electrical signal [14, 15], and the electrical signal has a certain linear relationship with the concentration of the sample to be measured. Due to the use of inexhaustible sunlight resources in nature, PEC sensors are expected to be used for commercial promotion in the future [16, 17].

However, how to achieve high sensitivity for BPA monitoring and specific identification of BPA using PEC sensors are quite critical and challenging issues. Recently, transition metal vanadate has been widely used in many emerging applications cover biosensors, photovoltaic conversion and catalysis due to their brilliant electronic, optical, and magnetic properties [18, 19]. CuV_2O_6 as an n-type semiconductor is a promising photoactive material with appropriate band gap (about 2 eV), low redox potential, and suitable chemical stability [20, 21]. However, the PEC properties of unmodified CuV_2O_6 are limited by the rapid complexation of photogenerated holes and electrons, which can greatly reduce the photocurrent signal [22]. It is a simple strategy to use a suitable sensitizer to sensitize CuV_2O_6 to improve the optical absorption capacity and facilitate the separation of photogenerated carriers, which could enhance the performance of the sensor. Chalcogenide compounds semiconductor have attracted plenty of research attention in recent years and they are increasingly used in academic research and industrial applications [23]. In particular, copper-based sulfide semiconductor materials have good photochemical properties. Ternary copper-based compound semiconductor of Cu_3BiS_3 is regarded as a promising compound for sensitizers, due to their narrow band gap [24], non-toxic, inexpensive, excellent layered structure, earth-abundant element, and ease of mass production [25, 26], making it stand out among many other materials. Moreover, the energy levels of Cu_3BiS_3 and CuV_2O_6 are matched to overlap in band structure, which can enhance the separation and transfer of photogenerated electrons. To enhance the selectivity of photocurrent sensors, DNA aptamers were employed as molecular recognition components. Aptamers can achieve high specificity and high affinity recognition, and they are more stable, easier to synthesize, and easier to modify on ITO glass electrode. For example, Yang et al. designed a ciprofloxacin photoelectrochemical aptasensor based on $Bi_{24}O_{31}Cl_{10}$/BiOCl heterojunction [27].

In this study, a novel PEC aptamer sensor was fabricated based on the unique advantages of the above materials with the aids of BPA aptamer. Scheme 1 shows the process of the above BPA aptasensor construction. When the photosensitive semiconductor material on the surface of the electrode is irradiated by visible light, photogenerated electrons and holes are produced. The electrons generated by the conduction band (CB) of the semiconductor are diverted to the electrode surface to produce the photocurrent. At the same time, the electron holes generated by the semiconductor valence band (VB) combine with the ascorbic acid (AA) in the electrolyte solution to generate a stable photocurrent. A series of performance tests showed that the PEC aptamer sensor in this paper has excellent PEC response and high sensitivity, which provides a viable solution for the detection of the BPA.

Experimental section

The materials and instruments employed in the experiment have been detailed in the Electronic Supporting Material (ESM).

Synthesis of Cu_3BiS_3

By referring to the previous literature, Cu_3BiS_3 was synthesized through hydrothermal synthesis [28]. The detailed synthetic procedures can be found in the ESM.

Synthesis of CuV_2O_6

CuV_2O_6 was synthesized via hydrothermal synthesis method [29]. The specific methods and procedures have been elaborated in the ESM.

The fabrication of PEC aptasensor

The PEC sensor was constructed on ITO glass, and the ITO electrode was cleaned with acetone, ethanol, and ultrapure water in the ultrasound machine, and then dryed at 70 °C in an oven. Next, 10 µL of Cu_3BiS_3 (5 mg/mL) solution was added dropwise to the bare ITO electrode for modification. After the first layer of material was dried in the ambient atmosphere, 10 µL of CuV_2O_6 (5 mg/mL) was dropped on the electrode and dried naturally. Next, 6 µL of (3 mM) thioglycolic acid (TGA) used to attach the BPA aptamer was modified on the surface of electrode. Afterward, 6 µL of BPA aptamer (5 µM) and 3 µL of BSA (1 wt%) were added on the electrode sequentially and dried at room temperature. Finally, the electrode was modified with 6 µL of BPA solution of different concentrations. When the ITO electrode dried naturally, the PEC sensing platform was obtained.

PEC performance detection

The PEC sensor performance was tested in PBS (0.1 M, pH = 8.0) buffer solution containing ascorbic acid (AA), where AA was used as a sacrificial electron donor in PEC measurement. The electrochemical impedance spectroscopy (EIS) test was performed in a mixture of phosphate buffer (pH = 8.0), 5.0 mmol/L $[Fe(CN)_6]^{-3/-4}$, and 0.1 mol/L KCl. Three-electrode system was composed of working electrode (the obtained PEC sensing platform), reference electrode (Hg/Hg_2Cl_2), and counter electrode (Pt). The PEC signal was measured by using current-time mode of the electrochemical work station at 0 V. By a certain program, the light source (400~700 nm) was employed as excitation light source, and it was switched on/off every 10 s.

Results and discussion

Analysis of the photoactive materials

The performance of the photoactive material plays an important role in the construction of the sensor, so the synthesized materials should be analyzed before characterizing the sensor properties. The crystal structure of Cu_3BiS_3 was characterized by X-ray diffraction (XRD). Comparing the characteristic peaks in the XRD pattern of Cu_3BiS_3 (Fig. 1A) with the standard card (PDF#: 43-1473) in the database, it can be seen that they have a high matching degree, which clearly shows that the preparation of Cu_3BiS_3 is successful. The scanning electron microscopy (SEM) image in Fig. 1B displays that Cu_3BiS_3 has a nanosheet structure; this unique sheet structure allows other materials to adhere to it more conveniently. Meanwhile, the photoactive materials were characterized by transmission electron microscopy (TEM). TEM image of Cu_3BiS_3 (Fig. 1C) manifests the typical lattice spacing with 0.207 nm, which can be attributed to the (2 1 0) crystal plane of the Cu_3BiS_3. The XRD pattern (Fig. 1D) of CuV_2O_6 indicates that CuV_2O_6 is successfully synthesized and all diffraction peaks of CuV_2O_6 are in good agreement with the standard card (PDF#: 43-0081). Figure 1E displays that CuV_2O_6 has a nanowire structure. As demonstrated in Fig. 1F, the 0.249-nm lattice spacing is consistent with the (2 0 6) facets of the CuV_2O_6.

To further determine the elemental composition and chemical state of the materials, X-ray photoelectron spectroscopy (XPS) of Cu_3BiS_3 and CuV_2O_6 was carried out. Figure 2A shows the basic element composition of Cu_3BiS_3. The high-resolution energy spectrum of Bi 4f and S 2p is shown in Fig. 2B; there are two strong characteristic peaks located at 158.82 eV and 164.14 eV, which attributed to S $2p_{3/2}$ and S $2p_{1/2}$ respectively [30]. The existence of characteristic peaks indicates that S element is in the state of S^{2-}, and the peaks of Bi $4f_{7/2}$ (158.78 eV) and $4f_{5/2}$ (164.75 eV) indicate the presence of the Bi^{3+} state in Cu_3BiS_3. As can be seen from Cu 2p spectrum (Fig. 2C), the binding energies of peaks at 932.35 eV and 952.42 eV represent the binding energies of Cu $2p_{3/2}$ and Cu $2p_{1/2}$. The value of the binding energy indicates that Cu is in the Cu^+ state. The same test was performed on CuV_2O_6. Figure 1D shows that the CuV_2O_6 is only composed of Cu, V, and O elements. Those two peaks observed at 516.88 eV and 524.36 eV are linked with V $2p_{3/2}$ and V $2p_{1/2}$ separately (Fig. 1E), suggesting the presence of V^{5+} within the CuV_2O_6 [31]. The characteristic peaks at 531.52 eV and 529.87 eV correspond to O 1s (Fig. 1F). The peaks of Cu $2p_{1/2}$ and Cu $2p_{3/2}$ are shown in

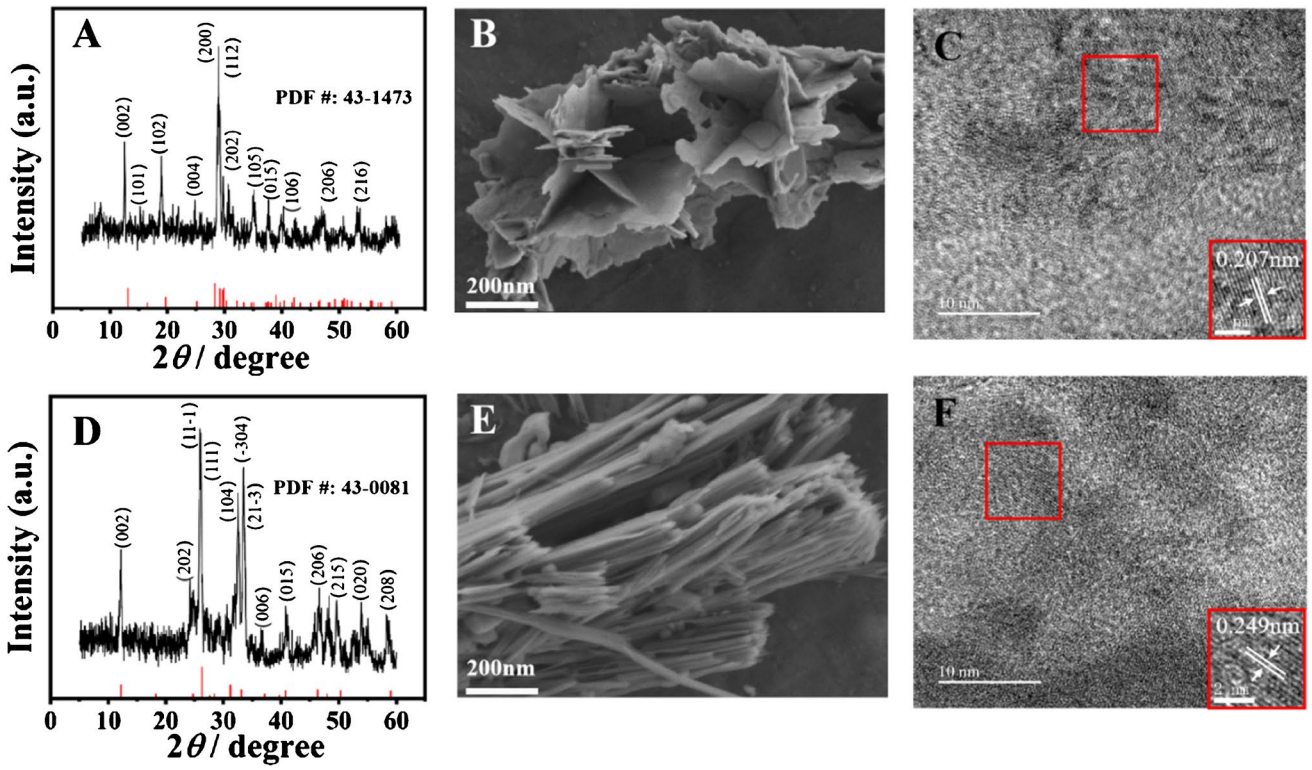

Fig. 1 The (**A**) XRD pattern, (**B**) SEM image, and (**C**) TEM image of Cu_3BiS_3. The (**D**) XRD pattern, (**E**) SEM image, and (**F**) TEM image of CuV_2O_6

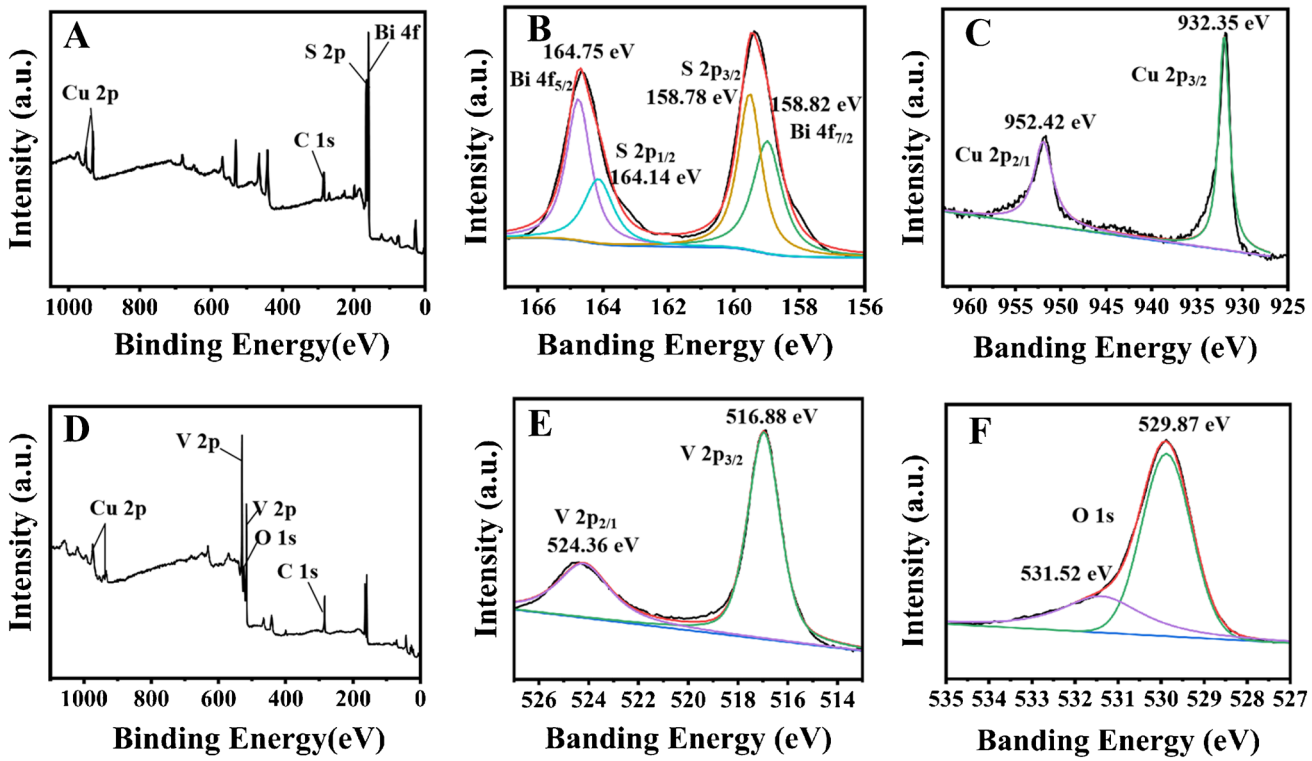

Fig. 2 **A** The XPS pattern of Cu_3BiS_3. The high-resolution energy spectrums of (**B**) Bi 4f and S 2p and (**C**) Cu 2p of Cu_3BiS_3. **D** The XPS pattern of CuV_2O_6. The high-resolution energy spectrums of (**E**) V 2p and (**F**) O 1s of CuV_2O_6

Fig. S1 (ESM file), and the binding energies of Cu $2p_{3/2}$ are located at 931.35 eV and 934.51 eV respectively. The peaks which locate at 951.89 eV and 954.92 eV belong to the Cu $2p_{1/2}$. The characterization results of the above materials prove the successful preparation of Cu_3BiS_3 and CuV_2O_6.

Optimal conditions for the experiment

In order to obtain a better PEC response and improve the performance of the constructed sensor, the effects of the pH of the PBS used for testing and the concentration of AA in the PBS were investigated. Corresponding data are given in the electronic support material. It can be seen from Fig. S2, pH of 8.0 and concentration of 0.1 M of AA in the test electrolyte were chosen as the best experimental conditions.

Possible charge transfer mechanism

By analyzing the band gap structure of the photovoltaic material, potential mechanisms for charge transfer in the PEC sensor can be uncovered. The band gap position and width of the material were measured by using linear scanning voltammetry and Mott-Schottky curves (Fig. S3). According to the relative positions of the valence and conduction bands of Cu_3BiS_3 and CuV_2O_6, these two materials form a type II heterostructure with staggered band gaps. Figure S4 illustrates the possible charge transfer mechanism in the constructed PEC sensor. Specific data and analytical processes are described in the ESM.

PEC performance characterization

To validate the successful construction of this PEC sensor, time-based photocurrent test was performed under the optimal experimental conditions. The plotting of time-photocurrent curves is one of the most effective means of describing the performance of the PEC sensors. As illustrated in Fig. 3A, during the construction of sensor, the photocurrent of the ITO electrode without any material modification was close to zero (curve a). Curve b shows that a certain photocurrent was obtained after modification with the photoactive material Cu_3BiS_3. The electrode was then modified with CuV_2O_6, and due to the two materials were well matched in band gap level, the photocurrent was increased (curve c). When the CuV_2O_6/Cu_3BiS_3 electrode was modified with TGA, aptamer of BPA and BSA, the response photocurrent decreased continuously (curve d, e). Finally, target BPA was modified on the electrode, and the lowest photocurrent value was measured (curve f). The reason for this change may be that the introduction of PBA inhibited charge migration on the electrode surface, which is called the steric hindrance effect. The BPA/BSA/aptamer/TGA/CuV_2O_6/Cu_3BiS_3 electrode showed a significant decrease in response photocurrent after modification with BPA, indicating that the aptamer sensor was sensitive and selective to BPA. The construction of the PEC aptamer sensor was proven successful.

The electrochemical impedance spectroscopy (EIS) is an excellent method used to measure the charge transfer resistance of sensors. Figure 3B compares the EIS patterns of several electrodes. The resistance value of the unmodified ITO glass was small (curve a), after Cu_3BiS_3 was added to the electrode, the resistance value increased (curve b). Next, when CuV_2O_6 was modified on the electrode, a larger resistance value was obtained (curve c). Subsequently, TGA, aptamer DNA, and BSA were modified on the electrode sequentially; the resistance increased continuously (curve d, e). Finally, BPA was modified on the electrode, and the largest charge transfer resistance was obtained (curve f). The gradual increase impedance values are consistent with

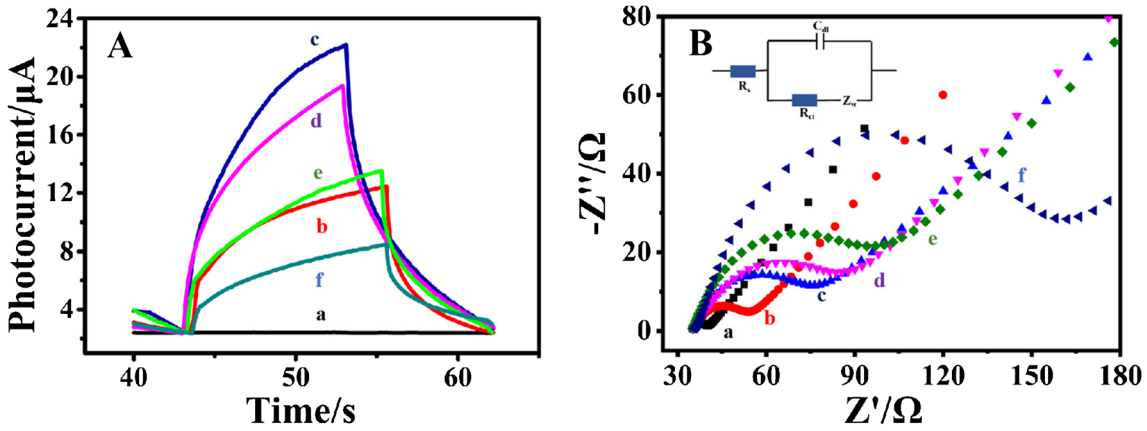

Fig. 3 **A** PEC responses of different electrodes and (**B**) EIS spectra of (a) ITO, (b) Cu3BiS3/ITO, (c) CuV_2O_6/Cu_3BiS_3/ITO, (d) aptamer/TGA/CuV_2O_6/Cu_3BiS_3/ITO, (e) BSA/aptamer/TGA/CuV_2O_6/Cu_3BiS_3/ITO, and (f) BPA/BSA/aptamer/TGA//CuV_2O_6/Cu_3BiS_3/ITO (cBPA = 200 ng/mL)

the time-photocurrent results, again demonstrating that .the modification of the electrode layers was successful.

Analytical properties of BPA

To test the performance of the constructed sensors, the photocurrent intensity of the sensor was tested under diverse concentrations of BPA. As the BPA concentration (0.5–50000 ng/mL) increased, the response photocurrent decreased (Fig. 4A). The linear equation between response photocurrent and BPA concentration is as follows: $I = 8.000 - 1.217\log c$ (ng/mL) ($R^2 = 0.9909$). The sensor also has a detection limit of 1.60×10^{-1} ng/mL ($S/N = 3$), showing a wide linear range and good potential application for BPA detection (Fig. 4B). The comparisons with the previously reported BPA sensors are indicated in Table S1. To verify the performance of the constructed sensor in other aspects, it is necessary to test the stability, repeatability, and selectivity of the designed sensor. Figure 4C shows that the PEC sensor is irradiated for 400 s without interruption, and tested for nearly 20 cycles of photocurrent test cycling. The photocurrent response of the sensor is hardly varied, which proves that the sensor is extremely stable. In addition, five ITO electrodes were prepared and measured independently, and the relative standard deviation (RSD) obtained was 3.1% (Fig. 4D), demonstrating that the reproducibility of the constructed aptasensor is excellent. Four different interfering substances were selected (including Ph, Py, 1-NP, 4-MP) for selective and interference-resistant experiments on the sensor. Selectivity experiments were conducted under conditions where the interference substance concentrations were the same. The results, as shown in Fig. S5A, indicate that the current signal strengths for Ph, Py, 1-NP, and 4-MP are 11.06%, 5.22%, 9.98%, and 3.84% of BPA, respectively, demonstrating good selectivity of the sensor to BPA. The interference resistance of the PEC sensor was analyzed by adding interfering substances, as shown in Fig. S5B, and due to the specific recognition of BPA by the ligand, the added interfering substances had virtually no effect on the photocurrent generated by the electrode.

Sample analysis

In order to verify the application potential of the as-prepared sensor in actual sample detection, the concentrations of BPA in water samples (ultrapure water, tap

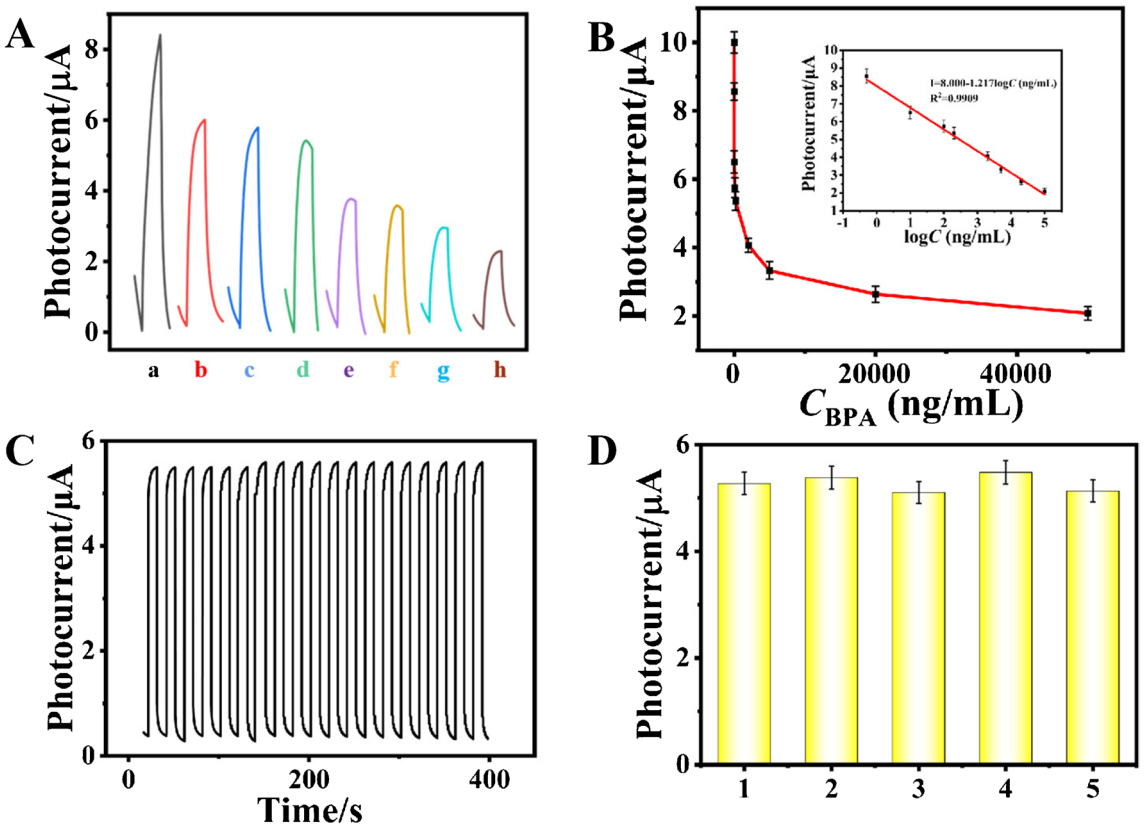

Fig. 4 The performance analytic of the BPA. **A** Photocurrent response of different concentrations of BPA (**B**) corresponding calibration curve of the PEC aptasensor: (from a to h) 0.5, 10, 100, 200, 2000, 5000, 20000, 50000 ng/mL. **C** Stability analysis and (**D**) reproducibility analysis (c_{BPA} = 200 ng/mL). Error bars: ± standard deviation (SD) (n = 3)

water, drinking water, and lake water) and soil sample were tested. Specific treatments of actual samples and selection of analyte addition concentrations are shown in the ESM. The designed sensors were also evaluated using standardized high performance liquid chromatography (HPLC) methods, and the test results are shown in Table S2, from which it can be seen that the RSD of the test results was less than 4%. The results suggest that the CuV_2O_6/Cu_3BiS_3-based BPA aptamer sensor is feasible for the detection of BPA in real samples, and indicate that the proposed method is promising for practical application.

Conclusion

In conclusion, an effective and simple CuV_2O_6/Cu_3BiS_3-based PEC aptamer sensor was proposed for the determination of BPA. The bandgap of the two materials is matched with a synergistic effect, which improves the sensitivity of the sensor. The selectivity of the sensor is enhanced through the application of an aptamer. Meanwhile, this method offers a wide linear range, effective stability, low detection limits, and is cost-effective for detecting BPA. Nevertheless, the suggested sensor has some limitations, such as low detection efficiency. Therefore, further improvements are necessary to enable the detection of multiple targets in the future. In conclusion, this sensing strategy provides a feasible idea and method for detecting BPA, and it is expected to have extensive application in safeguarding both environmental and food safety.

Supplementary Information The online version contains supplementary material available at https://doi.org/10.1007/s00604-023-06144-9.

Funding This study was supported by the National Natural Science Foundation of China (No. 22274062, 22206056); the Natural Science Foundation of Shandong Provincial (No. ZR2022QB117, No. ZR2020QB097, No. ZR2020QB072); the Science and Technology Program of the University of Jinan (No. XBS2108); and the Special Foundation for Taishan Scholar Professorship of Shandong Province.

Data Availability The data are available from the corresponding author on reasonable request.

Declarations

Conflict of interest The authors declare no competing interests.

References

1. Kaur B, Srivastava R, Satpati B (2015) Silver nanoparticle decorated polyaniline-zeolite nanocomposite material based nonenzymatic electrochemical sensor for nanomolar detection of lindane. RSC Adv 71:557657–557665
2. Ozyildiz G, Olmez-Hanci T, Arslan-Alaton I (2019) Effect of nano-scale, reduced graphene oxide on the degradation of bisphenol A in real tertiary treated wastewater with the persulfate/UV-C process. Appl Catal B 254:135–144
3. Verma D, Yadav A, Mukherjee M, Solanki P (2021) Fabrication of a sensitive electrochemical sensor platform using reduced graphene oxide-molybdenum trioxide nanocomposite for BPA detection: an endocrine disruptor. J Environ Chem Eng 910:550
4. Vandenberg L, Maffini M, Sonnenschein C, Rubin B, Soto A (2009) Bisphenol-A and the great divide: a r4.eview of controversies in the field of endocrine disruption. Endocr Rev 30:75–95
5. Karrer C, Boer W, Delmaar C, Cai Y, Crépet A, Hungerbühler K (2019) Linking probabilistic exposure and pharmacokinetic modeling to assess the cumulative risk from the bisphenols BPA, BPS, BPF, and BPAF for Europeans. Environ Sci Technol 53:9181–9191
6. Jiang D, Du X, Zhou L, Li H, Wang K (2018) TiO_2 nanoparticles embedded in borocarbonitrides nanosheets for sensitive and selective photoelectrochemical aptasensing of bisphenol A. J Electroanal Chem 818:191–197
7. Wang Y, Liang Y, Zhang S, Wang T, Zhuang X, Tian C (2021) Enhanced electrochemical sensor based on gold nanoparticles and MoS_2 nanoflowers decorated ionic liquid-functionalized graphene for sensitive detection of bisphenol A in environmental water. Microchem J 161:105769
8. Yang H, Wang B, Liu J, Cheng J, Yu L, Yu J (2020) Sensitive and selective detection of bisphenol compounds in a fluorescent metal-organic framework. Sens Actuators B Chem 314:128048
9. Zou J, Liu Z, Guo Y, Dong C (2017) Electrochemical sensor for the facile detection of trace amounts of bisphenol A based on cyclodextrin-functionalized graphene/platinum nanoparticles. Anal Methods 9:134–140
10. Huang C, Wu Y, Chen J, Han Z, Wang J, Pan H, Du M (2012) Synthesis and electrocatalytic activity of 3Au-1Pd alloy nanoparticles/graphene composite for bisphenol A detection. Electroanalysis 24(6):1416
11. Lu B, Liu M, Shi H, Huang X, Zhao G (2013) A novel photoelectrochemical sensor for bisphenol a with high sensitivity and selectivity based on surface molecularly imprinted polypyrrole modified TiO_2 nanotubes. Electroanalysis 25(3):771–779
12. Yue Z, Lisdat F, Parak W, Hickey S, Tu L, Sabir N (2013) Quantum-dot-based photoelectrochemical sensors for chemical and biological detection. ACS Appl Mater Interfaces 5:2800–2814
13. Zhao W, Shan S, Ma Z, Wan L, Xu J, Chen H (2013) Acetylcholine esterase antibodies on BiOI nanoflakes/TiO_2 nanoparticles electrode: a case of application for general photoelectrochemical enzymatic analysis. Anal Chem 85:11686–11690
14. Wang H, Xu Y, Xu D, Chen L, Qiu X, Zhu Y (2022) Graphitic carbon nitride for photoelectrochemical detection of environmental pollutants. ACS Est Eng 2:140–157
15. Zhao W, Xu J, Chen H (2015) Photoelectrochemical bioanalysis: the state of the art. Chem Soc Rev 44:729–741
16. Mao L, Ji K, Yao L, Xue X, Wen W, Zhang X (2019) Molecularly imprinted photoelectrochemical sensor for fumonisin B_1 based on GO-CdS heterojunction. Biosens Bioelectron 12757:63
17. Peng J, Huang Q, Liu Y, Liu P, Zhang C (2019) Photoelectrochemical sensor based on composite of cdte and nickel tetraamined phthalocyanine covalently linked with graphene oxide for ultrasensitive detection of curcumin. Sens Actuators B Chem 294:157–165
18. Kesavan G, Vinothkumar V, Chen S (2021) Sonochemical synthesis of copper vanadate nanoparticles for the highly selective voltammetric detection of antibiotic drug ornidazole. J Alloy Compd 867:159019

19. Zhou L, Yan Q, Yu J, Jones R, Becerra-Stasiewicz N, Suram S (2016) Stability and self-passivation of copper vanadate photoanodes under chemical, electrochemical, and photoelectrochemical operation. Phys Chem Chem Phys 18:9349–9352
20. Sivakumar V, Suresh R, Giribabu K, Manigandan R, Munusamy S, Kumar S (2014) Copper vanadate nanoparticles: synthesis, characterization and its electrochemical sensing property. J Mater Sci Mater Electron 25:1485–1491
21. Seabold J, Neale N (2015) All first row transition metal oxide photoanode for water splitting based on $Cu_3V_2O_8$. Chem Mater 27:1005–1013
22. Morcoso D, Franch A, Cardona I, Gimenez S (2017) Chromium doped copper vanadate photoanodes for water splitting. Catal Today 290:65–72
23. Manimozhi T, Archana J, Navaneethan M, Ramamurthi K (2019) Shape-controlled synthesis of $AgBiS_2$ nano-/microstructures using PEG-assisted facile solvothermal method and their functional properties. Appl Surf Sci 487:664–673
24. Hussain A, Luo J, Fan P, Liang G, Su Z, Ahmed R (2020) P-type Cu_3BiS_3 thin films for solar cell absorber layer via one stage thermal evaporation. Appl Surf Sci 505:144597
25. Gassoumi A, Musa M, Alfaify S, Nasr T, Bouarissa N (2017) The investigation of crystal structure, elastic and optoelectronic properties of $CuSbS_2$ and $CuSbS_2$ compounds for photovoltaic applications. J Alloy Compd 725:181–189
26. HuangD LL, Wang K, Li L, Feng K, Jiang F (2021) Wittichenite semiconductor of Cu_3BiS_3 films for efficient hydrogen evolution from solar driven photoelectrochemical water splitting. Nat Commun 12:3795
27. Yang M, Chen Y, Yan P, Dong J, Duan W, Xu L, Li H (2021) A photoelectrochemical aptasensor of ciprofloxacin based on $Bi_{24}O_{31}Cl_{10}$/BiOCl heterojunction. Microchim Acta 188:289
28. Kamimura S, Beppu N, Sasaki Y, Tsubota T, Ohno T (2017) Platinum and indium sulfide-modified Cu_3BiS_3 photocathode for photoelectrochemical hydrogen evolution. J Mater Chem A 5:10450–10456
29. Jansi Rani B, Ravi G, Yuvakkumar R, Praveen Kumar M, Ravichandran S, Velauthapillai D (2020) Photoelectrochemical activity of copper vanadate nanostructures. Mater Lett 274:127996
30. Martínez J, Díaz D, Herrera D, Rodríguez F, Pal M (2021) Theoretical evaluation of emerging Cd-free Cu_3BiS_3 based solar cells using experimental data of chemically deposited Cu_3BiS_3 thin films. J Alloy Compd 867:159156
31. Dong B, Sun T, Jiang X, Guo P, Yang G, Wang F (2021) Self-passivated CuV_2O_6 as a universal photoelectrode material for reliable and accurate photoelectrochemical sensing. Chem Commun 57:7402–7405